ORIGINAL PAPER

Anomalous lithium ion diffusion into CeO$_2$·TiO$_2$ thin film by film thickness variations

Chang-Yeoul Kim · Sung-Geun Cho · Tae-Young Lim · Duck-Kyun Choi

Abstracts CeO$_2$·TiO$_2$ thin film is considered as an excellent candidate for a passive ion storage layer due to its good electrochemical stability and comparatively great charge capacitance. When cerium-titanium oxide thin film is adopted as an ion storage layer against cathodic tungsten oxide layer, the electrochromic device shows long term durability and cyclability. Therefore, many researchers investigated the composition and crystallinity effects to the charge density. In our study, we prepared CeO$_2$·TiO$_2$ thin by sol–gel dip-coating method, varying thickness by controlling withdrawal speeds. As investigating results of cyclic voltammetry and chronocoulometry, we found that there are three regions in the film thicknesses: (1) fast lithium ion diffusion region under 100 nm, (2) slow diffusion region in the range of 100 to 150 nm, and (3) fast and great charge capacitance region over 150 nm. In region 1, lithium ions diffuse very fast and reach into indium-tin oxide (ITO) layers, and slow diffusion region follows in region 2, probably due to the remains or impurities within the film, and in region 3, lithium ion diffusion gets fast again, accompanied with charge capacitance increase with thickness.

C.-Y. Kim (✉) · S.-G. Cho
Nanomaterials Team,
Korea Institute of Ceramic Engineering & Technology,
233-5 Gasan-dong Geumcheon-gu,
153-801 Seoul, Korea
e-mail: cykim15@kicet.re.kr

S.-G. Cho · D.-K. Choi
Department of New Material Engineering, Hanyang University,
17 Haendang-dong Seongdong-gu,
133-791 Seoul, Korea

T.-Y. Lim
Glass & Display Team,
Korea Institute of Ceramic Engineering & Technology,
233-5 Gasan-dong Geumcheon-gu,
153-801 Seoul, Korea

Introduction

Electrochromic device is comprised of an electrochromic active layer, an electrolyte, and an ion storage layer. Electrochromic active layer is an active layer which inserts or extracts ions to result in the coloration and bleaching. Ion storage layer plays a role to receive and store proton or lithium ion to help an electrochromic layer to have an electrochemical stability and long cycle durability. Ion storage layer is divided into two categories, an active electrochromic ion storage which shows color change during insertion and extraction of ions like NiO$_2$ and a passive ion storage layer which shows no color change and acts as an only ion storage like CeO$_2$·TiO$_2$ [1–4].

CeO$_2$·TiO$_2$ thin film has been widely researched because it has a good electrochemical stability and long cycle durability. Baudry et al. [1] first reported about the electrochemical properties of CeO$_2$·TiO$_2$ thin film and suggested that small-size titanium ion substitution to large-size cerium sites gives an easy lithium ion insertion and higher diffusion coefficient than cerium oxide. Verma et al. [3] published their reports about the performance of CeO$_2$·TiO$_2$ as an ion storage layer with variations of Ce:Ti ratio. They presented that 1:1 composition of CeO$_2$:TiO$_2$ displayed the enhanced ion storage capacity in consequence of the increased disorderdness induced due to enhanced proportion of TiO$_2$ [3, 4]. Another composite ion storage layer with CeO$_2$, like V$_2$O$_5$–CeO$_2$, was also studied [5–9].

The electrochemical kinetics of $CeO_2 \cdot TiO_2$ was also reported [10]. However, there is no report about the film thickness effects to the ion storage capacitance.

In this research, we coated $CeO_2 \cdot TiO_2$ thin film prepared by sol–gel coating method with variations of the film thickness. We controlled the film thickness and evaluated the effects of film thickness to an ion storage capacitance. This research may be helpful to adopt $CeO_2 \cdot TiO_2$ thin film as an ion storage layer for electrochromic smart window system.

Experimental procedure

The synthesis of coating solution and thin film of $CeO_2 \cdot TiO_2$

The starting materials are cerium acetate hydrate (($C_2H_3O_2)_3Ce \cdot xH_2O$) and titanium tetraisopropoxide ($[(CH_3)_2CHO]_4Ti$). Cerium acetate hydrate was mixed with ethyl alcohol for 30 min and then titanium tetraisopropoxide was added to that solution. A small amount of HNO_3 was added to solve the remaining hydroxide during the reaction. The molar concentrations of cerium acetate hydrate and titanium tetraisopropoxide were 0.25 and 0.25, respectively to obtain 1:1 ratio of Ce:Ti.

$CeO_2 \cdot TiO_2$ thin film was coated on indium-tin oxide (ITO) glass substrate by dip-coating method. ITO glass substrate was dipped into the coating solution, held for 5 s, and then withdrawn at constant speeds varying from 50 to 200 mm min^{-1}. The coated film on ITO glass substrate was dried at 100 °C for 10 min and then heat treated at 200–600 °C for 1 h. $CeO_2 \cdot TiO_2$ thin film which was heat treated at 300 °C for 1 h was used for the characterization of electrochemical properties, because heat treatment at above 400 °C increased the resistance of ITO thin film.

Electrochemical analysis of $CeO_2 \cdot TiO_2$ thin film

1. Crystal structure and microstructure

X-ray diffraction analysis of $CeO_2 \cdot TiO_2$ thin film was conducted to investigate X-ray structure by X-ray diffractometer (KFX-987228-SE, Mac Science). Thicknesses of $CeO_2 \cdot TiO_2$ thin film were measured by observing cut-view images of the films by field-emission scanning electron microscopy (FE-SEM, JSM 6700, JEOL).

2. Electrochemical and electrochromic properties

Cyclic voltammetry and chronocoulometry were conducted to study the electrochemical properties of the films by PGASTAT 12 (AutoLab), and in situ optical transmittance was measured by 633 nm He–Ne laser (Newport 1830-C) while measuring the chemical properties simultaneously.

Results and discussion

Thickness variations of $CeO_2 \cdot TiO_2$ thin film with withdrawal speed and XRD analysis

Figure 1 shows XRD patterns of $CeO_2 \cdot TiO_2$ thin films with varied heat-treatment temperatures. $CeO_2 \cdot TiO_2$ thin films heat treated at 200–600 °C showed no crystalline peaks other than ITO crystalline peaks. $CeO_2 \cdot TiO_2$ thin film was amorphous until 600 °C. The changes of $CeO_2 \cdot TiO_2$ thin film thicknesses with withdrawal speeds were measured by FE-SEM as shown in Fig. 2. The cut-view images of $CeO_2 \cdot TiO_2$ thin films did not show any crystalline grains. The thickness variations with withdrawal speeds were also shown in Fig. 3. It increased linearly from 50 nm at 50 mm min^{-1} to 150 nm at 300 mm min^{-1}, and was 180 nm coated two times at 200 mm min^{-1}.

Electrochemical properties of $CeO_2 \cdot TiO_2$ thin film

Figure 4 shows cyclic voltammetry of $CeO_2 \cdot TiO_2$ thin films coated at various withdrawal speeds, which was measured from −2 to +2 V at a scan rate of 50 mV s^{-1}. When negative electrical potential was applied, lithium ion was intercalated into the film and the reduction current flowed. When positive electrical potential was applied, the current of oxidation flowed. The film coated at 50 mm min^{-1} had two reduction current peaks, −0.04 mA cm^{-2} at 0.15 V and −0.10 mA cm^{-2} at −0.735 V, and two oxidation current peaks, 0.05 mA cm^{-2} at 0.40 V and 0.142 mA cm^{-2} at 1.81 V. For the film coated at 100 mm min^{-1}, the reduction peaks were −0.03 mA cm^{-2} at 0.30 V and −0.163 mA cm^{-2} at −0.83 V and the oxidation peaks were 0.15 mA cm^{-2} at 0.78 V and 0.23 mA cm^{-2} at 1.41 V. The oxidation peaks and reduction peak currents were increased for the film coated at 100 mm min^{-1} compared to those for 50 mm
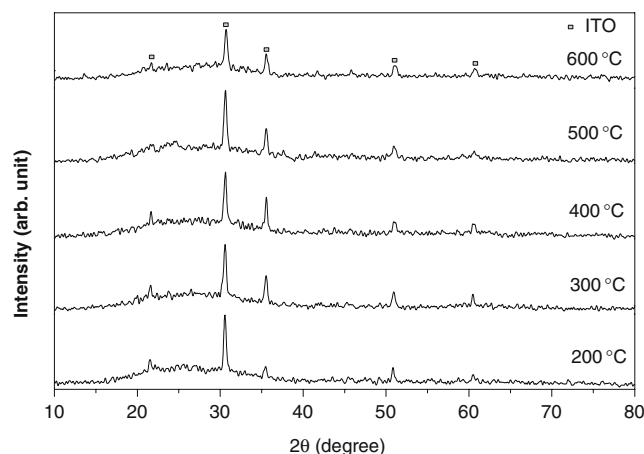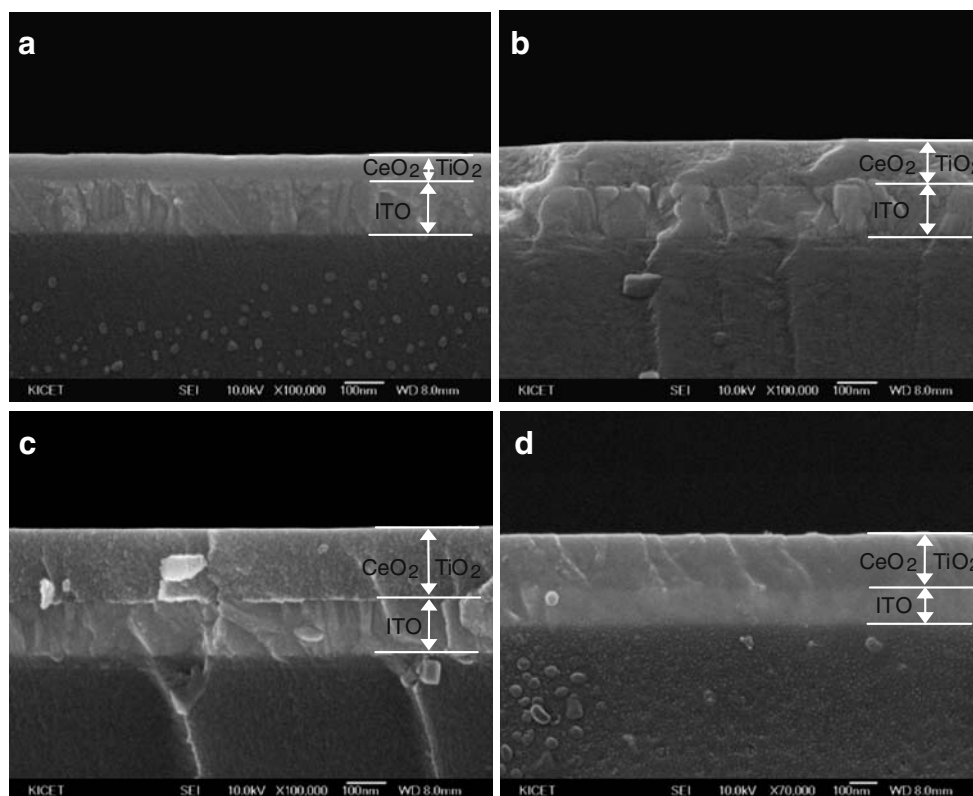

Fig. 1 X-ray diffraction patterns of cerium-titanium oxide thin film on ITO glass with various heating temperature layers

Fig. 2 FE-SEM vertical images of cerium-titanium oxide film prepared at different withdrawal speeds. **a** 100 mm min^{-1}, **b** 200 mm min^{-1}, **c** 300 mm min^{-1}, **d** 200 mm min^{-1}-2 layer

min^{-1}. However, when the film was coated at between 150 and 250 mm min^{-1}, the currents decreased, compared to those coated at 100 mm min^{-1}. The current peaks increase again when the film was coated at 300 mm min^{-1}. For the film coated at 200 mm min^{-1} for two cycles, the current peaks showed the maximum values, -0.183 mA cm^{-2} at -1.30 V for a reduction and 0.268 mA cm^{-2} at 1.46 V for an oxidation.

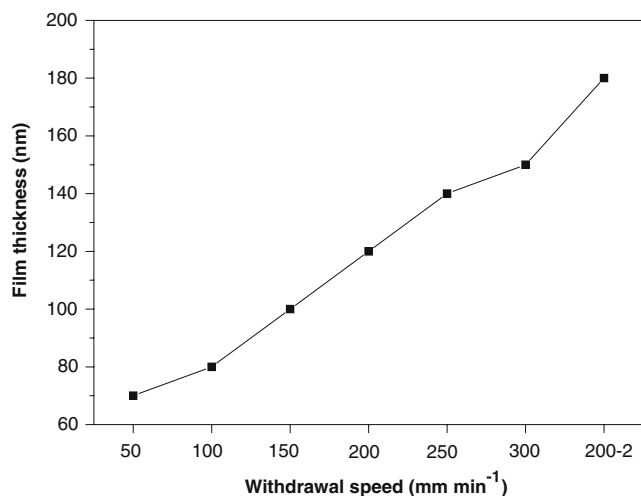The diffusion coefficients of the films with the thickness variations were shown in Fig. 5. The diffusion coefficients were calculated by using Randles and Sevicik equation [11].

$$I_p = 0.4463nF \left(\frac{nF}{RT}\right)^{1/2} CD^{1/2}v^{1/2} \tag{1}$$

Diffusion coefficient (D) can be calculated when we measure the cathodic and anodic current peak values. Here, n is the number of electrons involving the oxidation and the reduction, F is Faraday's constant (96,485 C mol^{-1}), C is the concentration of electrolyte (mol cm^{-3}), and v is the

Fig. 3 Thickness of CeO$_2$·TiO$_2$ thin film prepared at different withdrawal speed
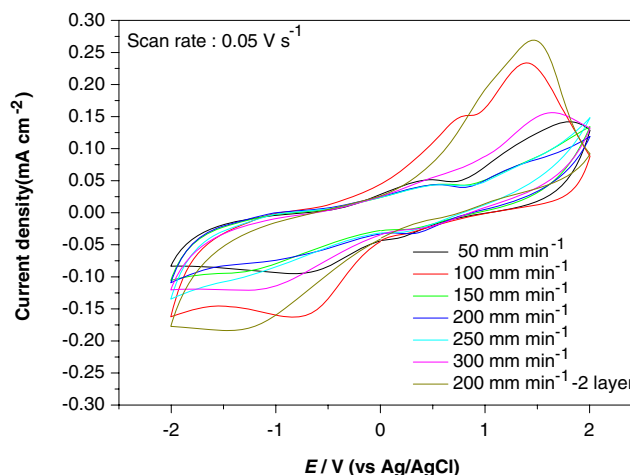

Fig. 4 Cyclic–voltammetric curves of cerium-titanium oxide thin films at different withdrawal speeds by dip-coating method
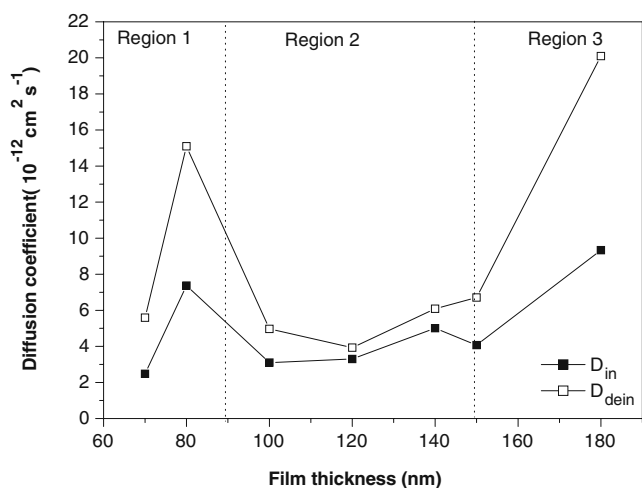
Fig. 5 Diffusion coefficient of Li$^+$ for cerium-titanium oxide thin film prepared at different withdrawal speeds

electrical potential sweep rate. The diffusion coefficients increased greatly from 2.5 and 5.7×10^{-12} cm^2 s^{-1} for intercalation and de-intercalation of 50 nm-thick film to 7 and 15×10^{-12} cm^2 s^{-1} for 80 nm-thick film. It decreased again to 3 and 5×10^{-12} cm^2 s^{-1} for intercalation and de-intercalation of the film with 100 nm thickness and slightly increased for 150 nm-thick film. For two-layer 200 mm min^{-1}-2 layer films with 180 nm thickness, D_{int} was 9.3×10^{-12} cm^2 s^{-1} and D_{deint} was 20.1×10^{-12} cm^2 s^{-1}. The diffusion coefficients are almost similar to those reported by Verma et al. [3]. The measurements on diffusion coefficient for Li$^+$ in DC magnetron-sputtered CeO$_{2x}$TiO$_2$ film was also performed by Janke et al. [12] using the cyclic voltammetric technique. The authors reported a value of 1.1×10^{-11} cm^2 s^{-1} at a scan rate of 10 mV s^{-1}. For a sputtered pure CeO$_2$ film, Baudry et al. [1] calculated the apparent diffusion coefficient of Li$^+$ to be equal to 3.9×10^{-13} cm^2 s^{-1} at 90 °C using the galvanostatic transient method. For the CeO$_2$ film, Keomany et al. [13] showed a diffusion coefficient value of 1.5×10^{-14} cm^2 s^{-1} at 80 °C. Using the sol–gel process, Tonazzi et al. [14] obtained an apparent diffusion coefficient value of 6.4×10^{-12} cm^2 s^{-1} at 25 °C, using the impedance spectroscopy for the Ce/Ti (1:1) composition. In the present study, the Ce/Ti (1:1) composition was endowed with a diffusion coefficient value of 9.44×10^{-12} cm^2 s^{-1} at 23 °C. It is evident from the values of apparent diffusion coefficients of Li$^+$ mentioned above that a better comparison is possible for the measurements on films deposited using the same technique for e.g., sol–gel process. They suggested that TiO$_2$ substitution generated CeO$_2$ nanocrystalline phase in amorphous TiO$_2$ matrix so that lithium ions could diffuse into nanocrystal-line CeO$_2$ phase rapidly. In this report, we fixed the molar ratio of CeO$_2$ and TiO$_2$. Therefore, we could say that there is no compositional difference of various thick CeO$_2 \cdot$TiO$_2$

thin films. Cerium-titanium oxide thin film with 80 nm thickness coated at 100 mm min^{-1} withdrawal speed showed the highest oxidation and reduction current density peaks. It is thought because lithium ion diffusion is the fastest in 80 nm-thick thin film, and the lithium ion diffusion coefficient decreased with increasing of thickness if the thickness is over 100 nm. The diffusion coefficient tended to increase slightly in the range of 100 and 160 nm. However, the thin film with 180 nm, coated two times at 200 mm min^{-1} withdrawal speed showed the largest coefficient values. It is thought to be from the facts that two times heat treatment removes the impurities like residuals and carbon within the thin film, and so there exist active sites to insert lithium ions.

Figure 6 showed charge densities of cerium-titanium oxide thin film coated at various withdrawal speeds measured by chronocoulometric method in 1 M LiClO$_4$-dissolved propylene carbonate liquid electrolyte when ±2 V was applied for 30 s. The charge densities are summarized in Tables 1 and 2. The cerium-titanium oxide thin film with 80 nm thickness showed the charge density of 5.8 mC cm^{-2} and it was increased to 7.1 mC cm^{-2} for 100 mm min^{-1}. It was decreased to 5.45 mC cm^{-2} for the film coated at 150 mm min^{-1} and decreased slightly to about 5 mC cm^{-2} at 250 mm min^{-1}. The film coated at 300 mm min^{-1} withdrawal speed recovered the charge density value of 7.2 mC cm^{-2}, similar to that of 100 mm min^{-1}. For 200 mm min^{-1}-2 layers, the charge density showed the maximum value of 9.4 mC cm^{-2}. As shown in Fig. 6, the charges were rapidly inserted for the thin film coated at below 100 mm min^{-1}. However, for the thin film coated at over 100 mm min^{-1}, the velocity of charge insertion became slow, which was known from the slope, and the charge densities got smaller. According to homogeneous ion diffusion mode, the
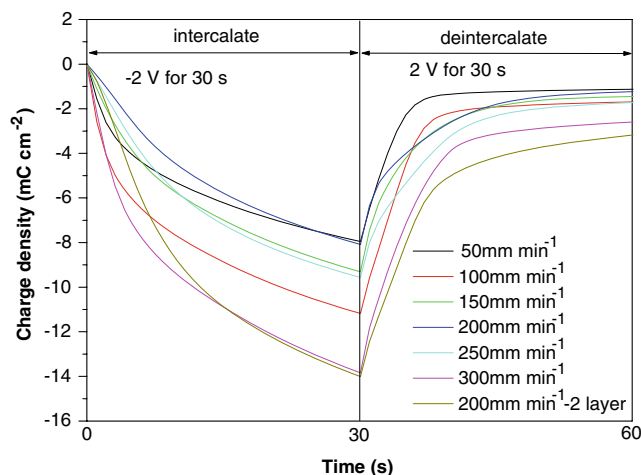

Fig. 6 Chronocoulometric curves (±2 V for each 30 s) for cerium-titanium oxide film prepared at different withdrawal speeds by dip-coating method

Table 1 Charge density, reversibility, and response time applied ±2V for each 30 s of cerium-titanium oxide thin film prepared at different withdrawal speeds by dip-coating method

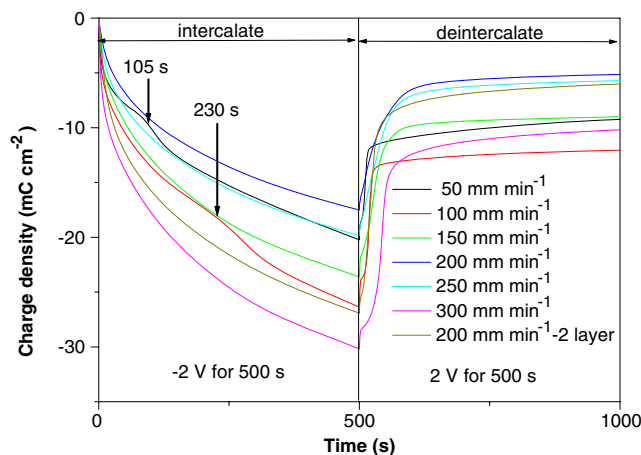|	Item				
	Charge density (mC cm^{-2})		Reversibility (%)	Response time (s)	
Conditions	In	Out		In	Out
50 mm min^{-1}	5.78	5.66	97.9	19	9
100 mm min^{-1}	7.11	6.94	97.6	20	10
150 mm min^{-1}	5.45	5.24	96.1	22	17
200 mm min^{-1}	5.09	4.88	95.9	22	21
250 mm min^{-1}	5.02	4.82	96.0	22	21
300 mm min^{-1}	7.20	6.99	97.1	21	15
200 mm min^{-1}-2 layer	9.43	9.28	98.4	12	15

Fig. 7 Chronocoulometric curves (±2 V for each 500 s) for cerium-titanium oxide film prepared at different withdrawal speeds by dip-coating method

cathodic current increases with film thickness. In this report, the lithium ion diffusion coefficient and charge densities are divided into three regions: (1) below 80 nm thickness region (withdrawal speed 100 mm min^{-1}), (2) the region between 100 and 150 nm thickness (withdrawal speed 150 mm min^{-1} and 250 mm min^{-1}), and (3) the region over 150 nm thickness (withdrawal speed 300 mm min^{-1} and 200 mm min^{-1}-2 layers). In region 1, the diffusion coefficient is greater and the lithium ions are rapidly inserted, compared to those in region 2. In region 2, the diffusion coefficient becomes smaller and the insertion occurs slowly, and they slightly increase with the increase in thickness. In region 3, they greatly increase with thickness variations. To investigate the anomalous behavior of charge density and insertion variations with thickness, we have done the chronocoulometry test for longer holding time of 500 s at ±2 V.

Figure 7 showed the charge densities measured at ±2 V for 500 s. The cerium-titanium oxide thin films coated at 50 and 100 mm min^{-1} have inflection points at 105 and 230 s,

Table 2 Charge density, reversibility and response time applied ±2 V for each 500 s of cerium-titanium oxide thin film prepared at different withdrawal speeds by dip-coating method

	Item				
	Charge density (mC cm^{-2})		Reversibility (%)	Response time (s)	
Conditions	In	Out		In	Out
50 mm min^{-1}	20.2	11.0	54.3	391	184
100 mm min^{-1}	26.4	14.3	54.2	376	36
150 mm min^{-1}	23.6	14.6	61.9	362	70
200 mm min^{-1}	17.5	12.4	70.7	370	108
250 mm min^{-1}	19.9	14.1	71.2	365	98
300 mm min^{-1}	30.2	20.0	66.3	343	114
200 mm min^{-1}-2 layer	26.9	20.9	77.7	356	82

respectively. We can calculate the diffusion length of lithium ion by using the Cottrell equation $i_d = nFc^o \frac{D^{1/2}}{(\pi t)^{1/2}}$. Here, i_d is diffusion current, n is the number of electrons involving the reaction, F is Faraday's constant, D is diffusion coefficient, and t is reaction time. In the equation, $(\pi Dt)^{1/2}$ is the quantity of length dimension and is considered as a diffusion length. The corresponding diffusion lengths are 50 nm for 70 nm-thick film coated at 50 mm min^{-1} and 100 nm for 80 nm-thick film coated at 100 mm min^{-1}, respectively. It indicates that lithium ion diffused through cerium-titanium oxide and reached the ITO layer. Lithium ion diffused into ITO is hard to extract from ITO thin film and might degrade the ITO film due to its weak chemical durability. The thicker film coated at more than 150 mm min^{-1} did not show the inflection point. The inserted charge density variations with the film
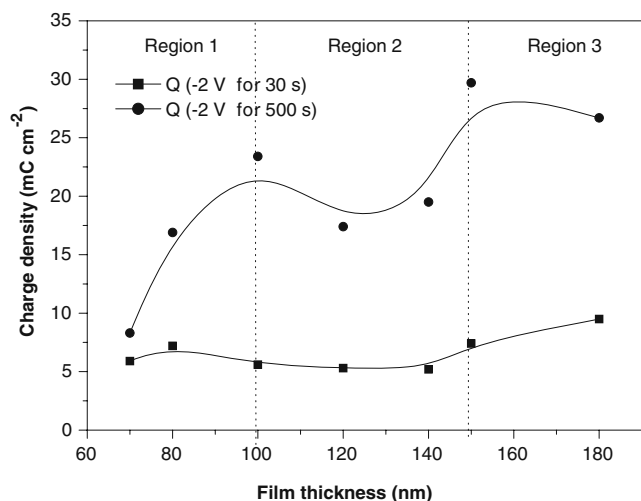

Fig. 8 Half cell charge capacitance of cerium-titanium oxide film **a** ±2 V for each 30 s and **b** for each 500 s and **c** film thickness at different withdrawal speeds by dip-coating method

thickness were shown in Fig. 8. The charge densities tended to increase with increasing thickness under 100 nm and began to decrease at 100 nm and maintained in the range of 100 and 140 nm and increased again. These results showed that there are three different types of lithium ion diffusion behaviors with film thickness variations. In region 1, fast ion diffusion occurs for $CeO_2 \cdot TiO_2$ thin film with below 80 nm thickness. In region 2, slow lithium ions diffuse in the range of 100–150 nm thickness. In region 3, fast lithium ions diffuse in over 150 nm-thick film. It is inferred that lithium ions diffuse very fast in region 1 because of whole removal of residuals in the film and more active sites for admitting lithium ions. However, in the range of 100–150 nm, there remain a lot of organic remains and impurities on which lithium ions impinge. As discussed in 200 mm min^{-1}-2 layers thin film, it indicates great diffusion coefficients and large capacitance density. It is one of the evidences which prove that two times heat treatment effectively removes impurities within thin film and increases active sites along with capacitance increase with film thickness.

Figure 8 shows the charge capacitance density changes with film thickness. As is shown in the figure, there exist three different regions of charge capacitances with film thickness variations. In region 1 below 100 nm, it indicated great charge capacitances and showed the tendency of increasing with thickness, and it became smaller in region 2 between 100 and 150 nm, and then large capacitance region 3 follows. Although we did not show the results of electrochromic device performance using various $CeO_2 \cdot TiO_2$ thin film in this report, the half cell test results tell us that $CeO_2 \cdot TiO_2$ thin film less than 100 nm is not suitable for an ion storage layer due to lithium ion diffusions into ITO. The most optimal thickness is over 150 nm, because it protects ITO transparent conducting film and provides great charge capacitance.

Conclusions

Anodic electrochromic layer of cerium-titanium oxide as an ion storage layer was dip coated onto ITO glass. We mainly investigated the electrochemical properties of the film by varying the film thickness. Cyclic voltammetry and chronocoulometry analysis results show that there are three

regions of lithium ion diffusions in different film thicknesses. (1) Lithium ion diffusion is very fast under 100 nm thickness in region 1, but lithium ion diffuses into ITO film under a long time of electrical potential which is not desirable for the application of electrochromic windows. (2) In region 2, between 100 nm and 150 nm thickness, diffusion coefficient decreases and lithium ions diffuse slowly and it has small charge densities, which is inferred from impurities remained within the film. (3) In region 3, fast ion diffusion and large charge capacitance behaviors appear again because film thickness increase provides large lithium ion sites and two times heat treatment effectively removes impurities.

References

1. Baudry P, Rodriguez ACM, Aegerter MA, Bulhoes LO (1990) J Non-Cryst Solids 121:319. doi:10.1016/0022-3093(90)90151-B
2. Camino D, Deroo D, Salardenne J, Treuil N (1995) Sol Energy Mater Sol Cells 39:349. doi:10.1016/0927-0248(95)00072-0
3. Verma A, Samanta SB, Mehra NC, Bakhshi AK, Agnihotry SA (2005) Sol Energy Mater Sol Cells 86:85. doi:10.1016/j.solmat.2004.06.008
4. Verma A, Singh DP, Bakhshi AK, Agnihotry SA (2005) J Non-Cryst Solids 351:2501
5. Šura A, Bencic S, Orel B, Pihlar B (1999) Electrochim Acta 44:3075–3084. doi:10.1016/S0013-4686(99)00023-7
6. Avellaneda CO, Bulhões LOS, Pawlicka A (2005) Thin Solid Films 471:100–104. doi:10.1016/j.tsf.2004.04.039
7. Rosario AV, Pereira EC (2002) Thin Solid Films 410:1–7. doi:10.1016/S0040-6090(02)00242-0
8. Yoshino T, Masuda H (2003) Solid State Ionics 165:123–129. doi:10.1016/j.ssi.2003.08.024
9. Berton MAC, Avellaneda CO, Bulhões LOS (2003) Sol Energy Mater. Cells 80:443. doi:10.1016/j.solmat.2003.08.012
10. Verma A, Samanta SB, Bakhshi AK, Agnihotry SA (2004) Solid State Ionics 171:81–90. doi:10.1016/j.ssi.2004.04.015
11. Randles JEB (1948) Trans Faraday Soc 44:327. doi:10.1039/tf9484400327
12. Janke N, Bieberle A, Weibmann R (2001) Thin Solid Films 392:134–141. doi:10.1016/S0040-6090(01)00898-7
13. Keomany D, Petit J-P, Deroo D (1995) Sol Energy Mater Sol Cells 36:397–408. doi:10.1016/0927-0248(94)00190-1
14. Tonazzi JCL, Valla B, Macedo MA, Baudry P, Aegerter MA, Rodriguez ACM et al (1990) SPIE Proc. 1328:375. doi:10.1117/12.22576